Zeeman Split Kramers Doublets in Spin-Supersolid Candidate $Na_2BaCo(PO_4)_2$

T. I. Popescu,[1] N. Gora,[1] F. Demmel,[2] Z. Xu,[3] R. Zhong,[4] T. J. Williams,[2] R. J. Cava,[4] G. Xu,[3] and C. Stock[1]
[1]School of Physics and Astronomy, University of Edinburgh, EH9 3JZ, United Kingdom
[2]ISIS Pulsed Neutron and Muon Source, STFC Rutherford Appleton Laboratory, Harwell Campus, Didcot, Oxon OX11 0QX, United Kingdom
[3]NIST Center for Neutron Research, 100 Bureau Drive, Gaithersburg, Maryland 20899, USA
[4]Department of Chemistry, Princeton University, Princeton, New Jersey 08544, USA

(Received 20 October 2024; revised 10 February 2025; accepted 28 February 2025; published 3 April 2025)

$Na_2BaCo(PO_4)_2$ is a triangular antiferromagnet that displays highly efficient adiabatic demagnetization cooling [Junsen Xiang *et al.*, Nature (London) **625**, 270 (2024)] near a quantum critical point at $\mu_0 H_c \sim 1.6$ T, separating a low-field magnetically disordered from a high-field fully polarized ferromagnetic phase. We apply high resolution backscattering neutron spectroscopy in an applied field to study the magnetic excitations near $\mu_0 H_c$. At large fields we observe ferromagnetic fluctuations that gradually transition to being overdamped in energy below $\mu_0 H_c$ where the magnetism is spatially disordered. We parametrize the excitations in the high-field polarized phase in terms of coupled Zeeman split Kramers doublets originating from the presence of spin-orbit coupling. On reducing the field, the splitting between the Kramers doublets is reduced and if done adiabatically, provides a mechanism for reducing temperature. On lowering the applied field through the $\mu_0 H_c$ the excitations characterize a textured phase that we suggest is inefficient for cooling. Low temperature disordered frustrated magnets built on Kramers doublets with nearby quantum critical points provide a route for efficient magnetocalorics.

DOI: 10.1103/PhysRevLett.134.136703

Low-dimensional magnets with frustrating interactions provide a platform for novel quantum phases and properties [1]. While the classical two-dimensional triangular antiferromagnetic displays 120° magnetic order, other exotic phases have been predicted to exist depending on the magnetic spin, including "hidden" nematic quadrupolar orders [2,3], disordered spin-liquid phases [4], and recently proposed spin supersolids [5–11] analogous to the supersolid phase sought after in solid helium [12]. Here we investigate the magnetic excitations in a candidate spin supersolid [13] and characterize the low temperature magnetic excitations as a function of magnetic field and discuss the response in terms of recently reported efficient adiabatic demagnetization cooling.

Antiferromagnetic triangular magnets can often be fully polarized with relatively small applied magnetic fields through a metamagnetic transition. [14] In terms of applications, the critical field separating a low-field disordered spin phase to a fully polarized state has been observed to host efficient magnetocaloric properties, making such systems candidates for adiabatic demagnetization [15,16]. In particular, $Na_2BaCo(PO_4)_2$ (NBCP) has been identified to display giant magnetocaloric properties [15]. NBCP consists of two-dimensional planes of coupled Co^{2+} ions [Fig. 1(a)] in a triangular arrangement resulting from a trigonal $P\bar{3}m1$ structure with lattice parameters $a = b = 5.3185$ Å and $c = 7.0081$ Å. Despite a Curie-Weiss constant of $|\Theta|_{CW} \sim 2$ K, magnetic order only appears at $T_N \sim 150$ mK with weak (reduced moment of $\mu \sim 0.5\ \mu_B$) incommensurate magnetic order [17,18]. On application of a magnetic field, this incommensurate magnetic order is replaced by an up-up-down $|\uparrow\uparrow\downarrow\rangle$ order with propagation wave vector $\vec{q}_0 = (1/3, 1/3)$ and has been proposed to host a spin-supersolid phase [19,20] supported by theoretical analysis of low-field neutron spectroscopy [21]. At large magnetic fields greater than $\mu_0 H_c \sim 1.6$ T, a fully polarized $|\uparrow\uparrow\uparrow\rangle$ magnetic state is present.

The critical magnetic field separating $|\uparrow\uparrow\downarrow\rangle$ and $|\uparrow\uparrow\uparrow\rangle$ phases has been found to display very efficient adiabatic demagnetization cooling [15]. In particular, reducing the field from large fields toward the critical field of $\mu_0 H_c \sim 1.6$ T has been found to reduce the temperature of the sample from a $T_0 = 2$ K to $T < 0.1$ K. However, for lower fields within the low field $|\uparrow\uparrow\downarrow\rangle$ phase warming is observed and eventual recovery of low temperatures found as the applied magnetic field is reduced to zero.

Cooling through adiabatic demagnetization involves splitting a ground state degeneracy with an applied magnetic field preferentially depopulating the energetically

costly excited states followed by lowering the field adiabatically (keeping relative populations constant). This can be understood through the Boltzmann distribution, $n(E) \propto e^{-\Delta E/k_b T}$, where demagnetization reduces ΔE, resulting in a lowering of the temperature of the system to maintain a constant particle number at each energy level $n(E)$. In this context, the foundation relevant for NBCP are the magnetic Co^{2+} ions coordinated in an octahedral environment. Given the multilevel quantum nature of demagnetization cooling, we first discuss the single-ion physics of isolated Co^{2+} ions in applied magnetic fields and then discuss experiments and data parametrization.

The magnetic Hamiltonian for Co^{2+} ions in NBCP can be divided into single-ion (SI) and interacting parts,

$$\mathcal{H} = \mathcal{H}_{\mathrm{SI}} + \sum_{ij} J(ij)\boldsymbol{S}(i)\cdot\boldsymbol{S}(j).$$

We first discuss the single-ion Hamiltonian $\mathcal{H}_{\mathrm{SI}}$. The hierarchy and effects of different terms in the single-ion Hamiltonian for Co^{2+} ($7d$-electrons) are illustrated in Fig. 1(b) [22]. The largest single-ion energy scale is the crystalline electric field $\mathcal{H}_{CEF}$ from an octahedral environment of oxygen that stabilizes a ground state spin-orbital triplet ($^4T_1$, Fig. 1) with an effective angular momentum of $l_{\mathrm{eff}} = 1$ and spin $S = 3/2$. [23] Given the presence of an orbital degeneracy, the next important term is spin orbit coupling $\mathcal{H}_{SO} = \alpha\lambda\vec{l}\cdot\vec{S}$ ($\alpha = -3/2$ is a projection factor [23,24]), which splits the spin-orbital states into three levels with total angular momentum $j_{\mathrm{eff}} = 5/2$, $3/2$, and a ground state $\frac{1}{2}$. The local octahedra surrounding the Co^{2+} site is distorted in NBCP and we parametrize this deviation of the crystalline electric field by a tetragonal distortion, $\mathcal{H}_{dis} = \Gamma[l_z^2 - (2/3)]$. The ground state degeneracy of the Kramers doublet is broken by a time reversal symmetry breaking field $\mathcal{H}_{MF} = h_{mf}S_z$ either by an applied magnetic field or a local molecular field from neighboring statically ordered spins.

In the following we parametrize the magnetic excitations extracted from neutron spectroscopy based on the single-ion eigenstates of $\mathcal{H}_{SI}$. We apply Green's response functions as the neutron scattering cross section is proportional to the imaginary part of the response function. This follows previous work applying this methodology to compounds with spin-orbit coupling [25–29], spin-only [30], and rare-earth [31] compounds and is outlined in Supplemental Material (SM) [32]. The calculations are based on mean-field theory applying the random phase approximation (RPA) [33]

$$G(\mathbf{Q},\omega) = g(\omega)[\mathbb{1} - \mathcal{J}(\mathbf{Q})g(\omega)]^{-1}$$

with single-site susceptibility $g(\omega)$ derived from the eigenstates of $\mathcal{H}_{\mathrm{SI}}$. The Fourier transform of the exchange constants is denoted as $\mathcal{J}(\mathbf{q})$.

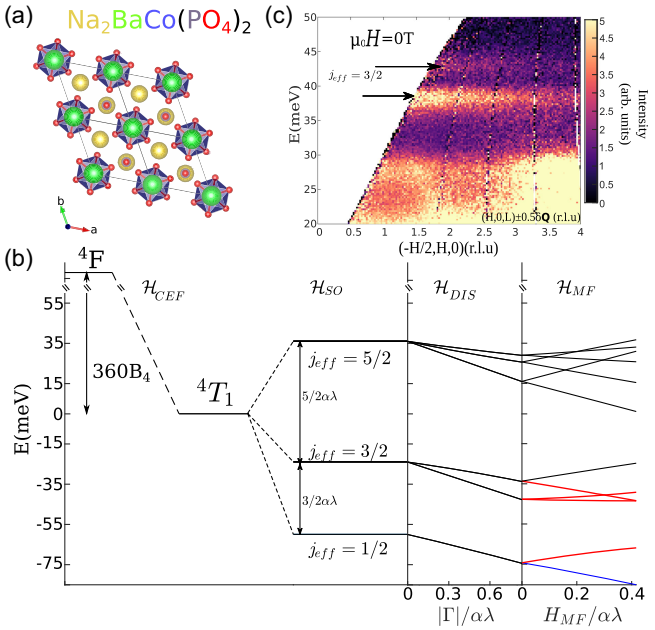

FIG. 1. (a) Structure of $Na_2BaCo(PO_4)_2$ (NBCP) with octahedral CoO_6. (b) Co^{2+} single-ion energies under spin-orbit, distortion and molecular field with an overall applied octahedral crystalline electric field. The dipole active quantum levels with finite neutron cross section from the ground state (blue) are highlighted in red. (c) Constant momentum slice (MAPS) at $T = 10$ K of the first spin-orbit level $j_{\mathrm{eff}} = 3/2$. We note that given the direction of the integration, the spectral intensities found at zero on the x-axis describe a sum over $(0, 0, \pm 0.5)$ rather than data strictly at the $|\vec{Q}| = 0$ origin.

Neutron spectroscopy was performed on OSIRIS [34] (ISIS, UK) with a coaligned NBCP sample mounted in a dilution fridge with (HK0) Bragg reflections in the horizontal plane. The elastic energy resolution with $E_f = 1.84$ meV is 0.025 meV (full width) [35]. While the mixing chamber was held at T = 50 mK, no evidence for static magnetism was observed and this taken with previous calibrations performed on heavy fermions [36,37] in similar configurations leads us to the conclusion the sample temperature was greater than ~100 mK. Vertical resolution defined by the detector geometry is estimated to be ±0.2 r.l.u along c^*. Higher energy data characterizing spin-orbit transitions were taken on the MAPS spectrometers. Further experimental details are given in the SM [32].

We now discuss our MAPS data [Fig. 1(c), $T = 10$ K], where the only terms that are expected to define $\mathcal{H}_{SI}$ are the distortion Γ and spin-orbit coupling λ. The dominant cross section in Fig. 1 (below ~30 meV) are phonons as the scattering increases with momentum transfer. Two distinct dispersionless bands near ~40 meV match the expected splitting of energy levels in Fig. 1(b) for excitations from the ground state $j_{eff} = \frac{1}{2} \rightarrow j_{eff} = 3/2$ manifold. As discussed in the SM [32], the intensity from these excitations decays with increasing momentum transfer and is

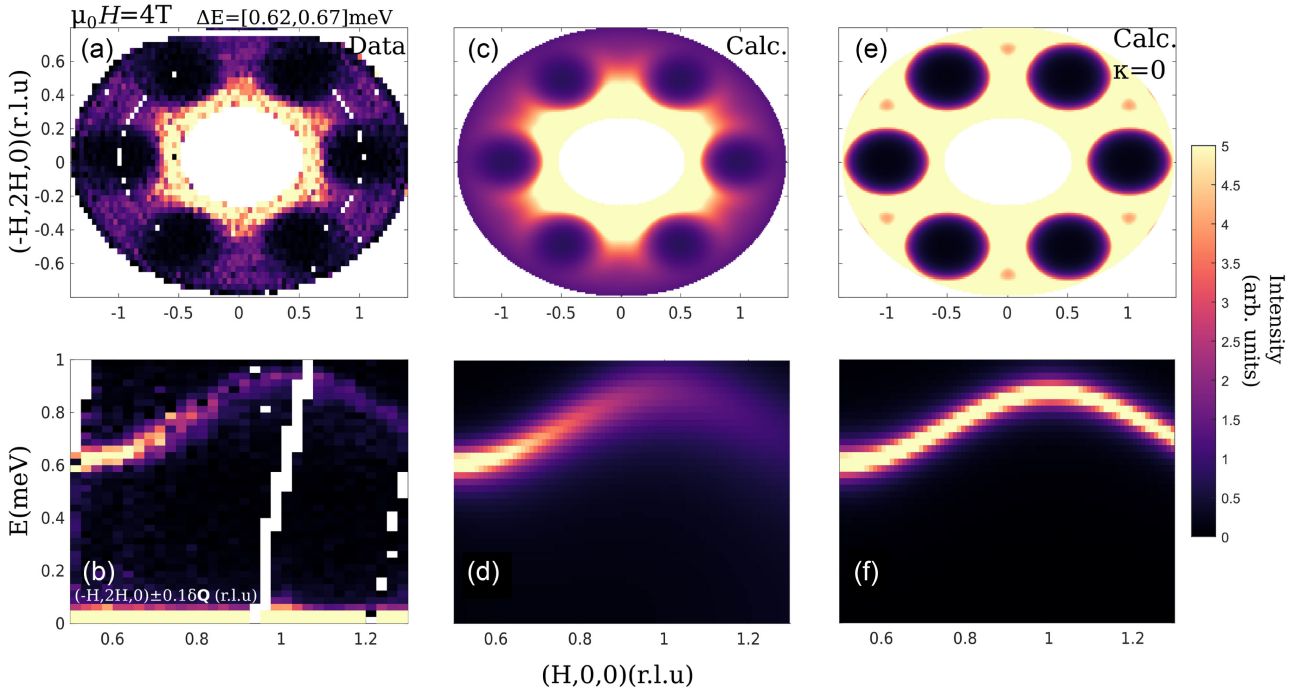

FIG. 2. Constant energy slices (OSIRIS) taken at 4 T from (a) the measured data between $\Delta E = [0.62, 0.67]$ meV, (c) RPA calculations with the inclusion of the term κ taken at E = 0.645 meV, and (e) RPA theory excluding κ. Constant momentum slices are also presented with (b) data cuts integrating along the $(-\mathrm{H} \pm 0.1,\ 2\mathrm{H} \pm 0.1, 0)$ direction. Additional RPA theoretical dispersion plots taken at $H = 0$ along the (H, 0, 0) direction (d) including the parameter κ and (f) excluding it.

described by the isotropic Co^{2+} form factor [38,39]. The energy position of these two modes fixes $\lambda = -18 \pm 2$ meV and $\Gamma = 10 \pm 2$ meV in $\mathcal{H}_{SI}$.

We now discuss the low-energy excitations within the $j_{eff} = \frac{1}{2}$ ground state and our parametrization of the magnetic excitations in the low-temperature fully spin-polarized $|\uparrow\uparrow\uparrow\rangle$ phase. Figures 2(a) and 2(b) illustrate constant energy and momentum slices through the magnetic excitations which disperse over the energy range of ~0.6–0.95 meV. We describe these in terms of single-ion Kramers doublets in Figs. 2(e) and 2(f) coupled with a nearest neighbor exchange coupling of $J = 0.0095$ meV via RPA. The calculated neutron response includes an isotropic Co^{2+} form factor found to describe the momentum dependent intensity of the single-ion excitations in Fig. 1(c). The derived exchange constant can be used to calculate a Curie-Weiss constant (assuming $j_{eff} = \frac{1}{2}$) of $|\Theta_{CW}| = 2$ K, which is in agreement with experiment. However, while the RPA [Figs. 2(e) and 2(f)] describes the magnetic dispersion and momentum dependence, it fails to describe the momentum dependent intensity (Figs. 2(a) and 2(b)], particularly at large momentum transfers near the zone boundary where the intensity in the data decreases faster with momentum transfer than would be expected from the isotropic Co^{2+} magnetic form factor.

To account for this decrease in intensity, we follow Refs. [40,41] and consider a distribution of response functions centered around the Green's response function predicted with the RPA calculation outlined above. To account for this and motivated by the imaginary-part self-consistent Born approximation (iSCBA) we include an additional parameter κ,

$$\mathcal{G}^{-1}(\mathbf{Q}, \omega) = G^{-1}(\mathbf{Q}, \omega) + i\kappa. \tag{1}$$

The extra term κ results in a broadening of the excitations. Following works on liquids [42] we assign a momentum dependence to this term that varies to leading order $\kappa = \xi|\mathbf{Q}|^2$, preserving even symmetry in momentum transfer. Inclusion of this heuristic parameter ξ that characterizes the distribution of Green's response functions is illustrated in Figs. 2(c) and 2(d) and accounts for the decrease of intensity with increasing momentum transfer. We discuss the field dependence of this parameter below. This additional term can be motivated by a mode-coupling analysis [43] which may result from the coupling of single-magnon excitations to another degree of freedom such as a multimagnon continuum. While the single and multimagnon dispersion relations do not kinematically intersect, the two processes are expected to become close energetically near the zone boundary, thereby potentially enhancing coupling.

The field dependence of the dispersive excitations is illustrated in Fig. 3. Decreasing applied magnetic fields of $\mu_0 H = 3$, 2 T is shown in Figs. 3(a) and 3(c), where the excitation energetic gap decreases. This is replicated in our

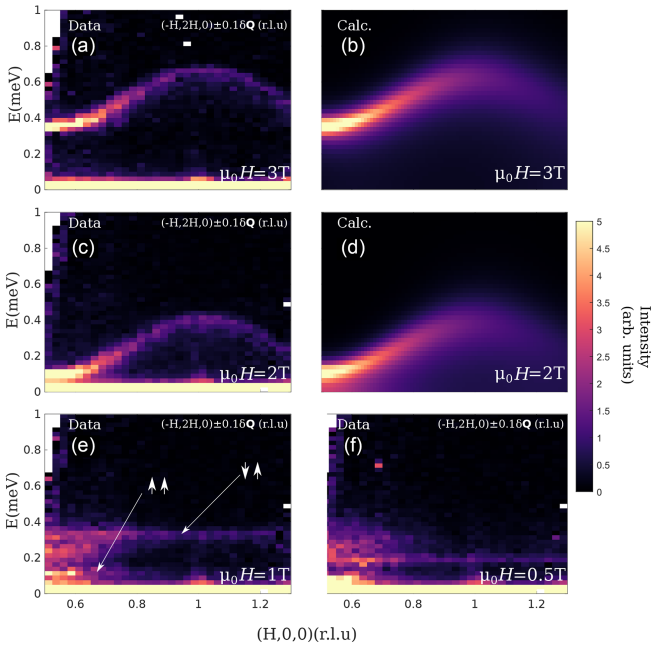

FIG. 3. Constant momentum slices (OSIRIS) integrating along $(-\mathrm{H}\pm 0.1, 2\mathrm{H}\pm 0.1, 0)$ for (a) $\mu_0 H = 3.0$ T, (c) 2.0 T, (e) 1.0 T, (f) 0.5 T. RPA calculations for (b) $\mu_0 H = 3.0$ T and (d) 2.0 T.

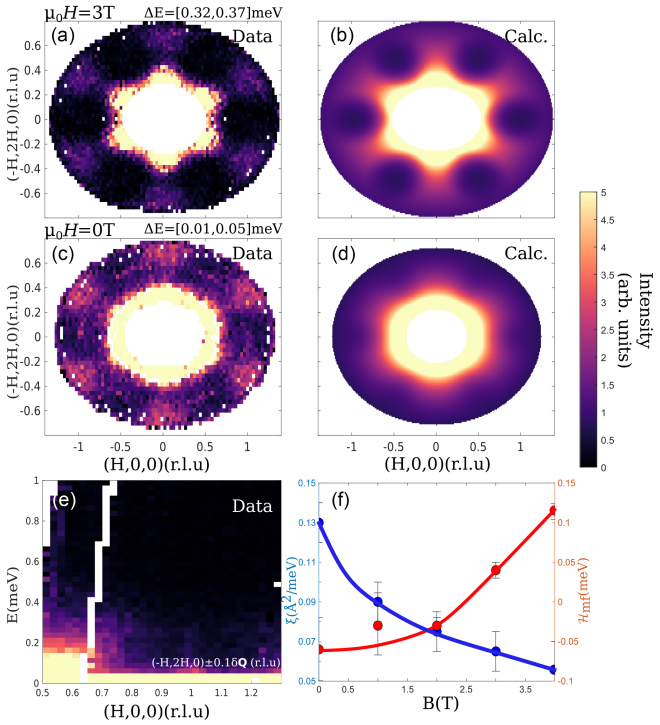

FIG. 4. Folded constant-E slices (OSIRIS) at (a) E = [0.32,0.37] meV (3 T) and (c) [0.01, 0.015] meV (0 T). RPA calculations at (b) E = 0.325 meV (3 T) and (d) 0.085 meV (0 T). (e) Constant-$\vec{Q}$ slice (OSIRIS) at $\mu_0 H = 0$ T. (f) Obtained parameters as a function of $\mu_0 H$ with guiding lines.

response theory in Figs. 3(b) and 3(d) and can be understood in terms of a decrease in splitting of the ground state $j_{eff} = \frac{1}{2}$ Kramers doublet illustrated in the single-ion response in Fig. 1(b). This originates from a combination of a decrease in the applied magnetic field and decrease of local magnetic order contributing to the molecular field term in Fig. 1(b). This reduced splitting of the ground state Kramers doublet, if performed adiabatically, keeping the relative population of the differing quantum levels fixed, will lead to cooling of the sample.

Below 2 T and illustrated in Figs. 3(e) and 3(f), the neutron response changes dramatically from leaving the fully polarized $|\uparrow\uparrow\uparrow\rangle$ phase to the intermediate $|\uparrow\uparrow\downarrow\rangle$ phase. Figures 3(e) and 3(f) are complex, consisting of correlated magnetic scattering near H ~ 0.5 r.l.u. and also two field dependent flat modes that soften as the field is lowered from 1 to 0.5 T. It is possible to attribute the two visible flat modes to pair spectra of nearest neighbor Co^{2+} ions. The higher energy flat mode in Figs. 3(e) and 3(f) can be assigned to a pair excitation of antialigned spins, with one of the spins experiencing a strong molecular field from its six nearest neighbors being aligned with the field. Meanwhile, the lower energy mode originates from a pair excitation of aligned spins, this lower energy originating from the spins not experiencing a molecular field. Both situations are expected to exist in the textured $|\uparrow\uparrow\downarrow\rangle$ phase. These excitations are indicative of a complex or textured order which may be expected given that Ising-like $|\uparrow\downarrow\rangle$ on a triangular motif is likely disordered. The complex and multilevel excitation spectrum is indicative of a large entropic ground state which is disordered. It is in this $|\uparrow\uparrow\downarrow\rangle$ phase that NBCP lacks cooling efficiency.

In Fig. 4 we compare constant energy slices in this intermediate phase [Figs. 4(a) and 4(c)] to our parametrization outlined in Figs. 4(b) and 4(d). On lowering the field and on comparing with Fig. 2, the momentum dependence in Figs. 4(a) and 4(c) becomes broader, indicative of a shortening of dynamic spatial correlations in the $|\uparrow\uparrow\downarrow\rangle$ and the $\mu_0 H = 0$ T phases. The loss of spatial correlations is particularly evident in Fig. 4(c) at small momentum transfers where the scattering nearly has lost the sixfold symmetry seen at higher applied fields and forms nearly a ring in momentum. Simultaneously, the temporal correlations [Fig. 4(e)] become extended at zero applied field. This relaxational-like scattering at $\mu_0 H = 0$ T is in contrast to the dispersive excitations discussed above in the polarized phase for fields in excess of $\mu_0 H_c$.

The momentum broadening is reproduced in our calculations in Figs. 4(b) and 4(d) by increasing the parameter κ which corresponds to a broader distribution of Green's functions discussed above. In Fig. 4(f) we plot the parameters ξ that characterizes the distribution of response functions and also the molecular field we have used as a function of applied magnetic field. There is a trade-off between the two parameters with a nearly fully saturated

molecular field found to reproduce the magnetic response at $\mu_0 H = 4$ T and minimal ξ. Indeed at small and zero applied magnetic fields where the ground state is disordered, there is a broad distribution of neutron response functions indicated by large values of ξ. As the polarized $|\uparrow\uparrow\uparrow\rangle$ phase is entered, the molecular field increases, indicative of the formation of the polarized and spatially correlated $|\uparrow\uparrow\uparrow\rangle$ phase. It is interesting to note that full saturation of the molecular field is not onset immediately above the critical applied field of $\mu_0 H_c \sim 1.6$ T and gradually forms with increased field, indicative of the second-order nature of the critical point. Concomitantly, the parameter ξ which is related to the distribution of neutron response functions κ decreases, indicative of a narrowing of the distribution of responses.

Our parametrization agrees with expectations based on the statics reported previously from diffraction and susceptibility. While magnetic order is observed at zero field, it is only a fraction of the expected total based on observations in other cobalt oxide compounds. This is indicative of a large fluctuating moment, corroborated by the low temperature $\mu_0 H = 0$ T response that we observed in Fig. 4(e). This largely disordered "liquid"-like phase is parametrized by a broad range of localized response functions in our analysis.

While the excitation spectrum at $\mu_0 H = 0$ T is broadened in both momentum and energy and lacks the strong dispersive nature of the excitations at high fields, it is less complex than intermediate fields in the $|\uparrow\uparrow\downarrow\rangle$ phase where a mixture of relaxational components near the magnetic zone center and dispersionless features were observed. This spectrum is noted to host more efficient cooling than in the intermediate $|\uparrow\uparrow\downarrow\rangle$ phase.

NBCP displays efficient cooling through adiabatic demagnetization. Based on our mapping and parametrization of the magnetic response discussed above, there are several reasons for this. The primary reason is a ground state Kramers doublet originating from the single-ion physics of Co^{2+} which can only be split in the presence of a time reversal symmetry breaking magnetic field. Kramers doublets cannot be split in a time reversal symmetry perserving field such as a crystalline electric field. Zeeman splitting for NBCP occurs for magnetic fields above $\mu_0 H_c = 1.6$ T. Normally for field induced critical points defining a low-field magnetically ordered phase, the Kramers doublet would split again at lower fields below the critical magnetic field characterized by an opening of an excitation gap [44–46].

This is noted in the $|\uparrow\uparrow\downarrow\rangle$ phase, where an effective splitting seen in Figs. 3(e) and 3(f) causes a rise in temperature. We note that owing to disorder in this intermediate field phase, there are excitations which are dispersionless, indicative of Co^{2+} sites which lack any molecular field or coupling and increases the entropy in this field range that causes heating. Meanwhile, at $\mu_0 H = 0$ T the liquid-like ground state preserves the Kramers ground state degeneracy and hence cools the sample. The two essential components for efficient cooling in NBCP are therefore the single-ion physics that provides the basis for the Kramers doublets and frustrated spin interactions preventing full spatially long-range magnetic order at zero field.

In summary we have applied high resolution neutron spectroscopy to study the correlated Kramers doublet magnetism near the field induced critical point $\mu_0 H_c \sim 1.6$ T. We have parametrized the excitations in terms of ground state $j_{eff} = \frac{1}{2}$ doublets coupled via the mean field random phase approximation. We have included a broadening parameter to account for a distribution of responses owing to the inherently disordered ground state. We have also mapped out the excitations in the low-field disordered and $|\uparrow\uparrow\downarrow\rangle$ phases.

Acknowledgments—We are grateful to the STFC and the EPSRC for support.

[1] M. F. Collins and O. A. Petrenko, Triangular antiferromagnets, Can. J. Phys. **75**, 605 (1997).
[2] H. Tsunetsugu and M. Arikawa, Spin nematic phase in S = 1 triangular antiferromagnets, J. Phys. Soc. Jpn. **75**, 083701 (2006).
[3] E. M. Stoudenmire, Simon Trebst, and Leon Balents, Quadrupolar correlations and spin freezing in S = 1 triangular lattice antiferromagnets, Phys. Rev. B **79**, 214436 (2009).
[4] P. W. Anderson, Resonating valence bonds: A new kind of insulator, Mater. Res. Bull. **8**, 153 (1973).
[5] Stefan Wessel and Matthias Troyer, Supersolid hard-core bosons on the triangular lattice, Phys. Rev. Lett. **95**, 127205 (2005).
[6] R. G. Melko, A. Paramekanti, A. A. Burkov, A. Vishwanath, D. N. Sheng, and L. Balents, Supersolid order from disorder: Hard-core bosons on the triangular lattice, Phys. Rev. Lett. **95**, 127207 (2005).
[7] Dariush Heidarian and Kedar Damle, Persistent supersolid phase of hard-core bosons on the triangular lattice, Phys. Rev. Lett. **95**, 127206 (2005).
[8] Massimo Boninsegni and Nikolay Prokof'ev, Supersolid phase of hard-core bosons on a triangular lattice, Phys. Rev. Lett. **95**, 237204 (2005).
[9] Dariush Heidarian and Arun Paramekanti, Supersolidity in the triangular lattice spin-1/2 XXZ model: A variational perspective, Phys. Rev. Lett. **104**, 015301 (2010).
[10] Fa Wang, Frank Pollmann, and Ashvin Vishwanath, Extended supersolid phase of frustrated hard-core bosons on a triangular lattice, Phys. Rev. Lett. **102**, 017203 (2009).
[11] H. C. Jiang, M. Q. Weng, Z. Y. Weng, D. N. Sheng, and L. Balents, Supersolid order of frustrated hard-core bosons in a triangular lattice system, Phys. Rev. B **79**, 020409(R) (2009).
[12] E. Kim and M. H. W. Chan, Probable observation of a supersolid helium phase, Nature (London) **427**, 225 (2004).
[13] Y. Gao, Y-C Fan, H. Li, F. Yang, X.-T Zeng, X.-L. Sheng, R. Zhong, Y. Qi, Y. Wan, and W. Li, Spin supersolidity in

nearly ideal easy-axis triangular quantum antiferromagnet $Na_2BaCo(PO_4)_2$, npj Quantum Mater. **7**, 89 (2022).
[14] E. Stryjewski and N. Giordano, Metamagnetism, Adv. Phys. **26**, 487 (1977).
[15] Junsen Xiang, Chuandi Zhang, Yuan Gao, Wolfgang Schmidt, Karin Schmalzl, Chin-Wei Wang, Bo Li, Ning Xi, Xin-Yang Liu, Hai Jin *et al.*, Giant magnetocaloric effect in spin supersolid candidate $Na_2BaCo(PO_4)_2$, Nature (London) **625**, 270 (2024).
[16] Chuandi Zhang, Junsen Xiang, Quanliang Zhu, Longfei Wu, Shanfeng Zhang, Juping Xu, Wen Yin, Peijie Sun, Wei Li, Gang Su, and Wentao Jin, Structural, magnetic, and magnetocaloric properties of triangular-lattice transition-metal phosphates, Phys. Rev. Mater. **8**, 044409 (2024).
[17] Jieming Sheng, Le Wang, Andrea Candini, Wenrui Jiang, Lianglong Huang, Bin Xi, Jize Zhao, Han Ge, Nan Zhao, Ying Fu *et al.*, Two-dimensional quantum universality in the spin-1/2 triangular-lattice quantum antiferromagnet $Na_2BaCo(PO_4)_2$, Proc. Natl. Acad. Sci. U.S.A. **119**, e2211193119 (2022).
[18] S. Lee, C. H. Lee, A. Berlie, A. D. Hillier, Devashibhai T. Adroja, Ruidan Zhong, R. J. Cava, Z. H. Jang, and K.-Y. Choi, Temporal and field evolution of spin excitations in the disorder-free triangular antiferromagnet $Na_2BaCo(PO_4)_2$, Phys. Rev. B **103**, 024413 (2021).
[19] R. Zhong, S. Guo, G. Xu, Z. Xu, and R. J. Cava, Strong quantum fluctuations in a quantum spin liquid candidate with a Co-based triangular lattice, Proc. Natl. Acad. Sci. U.S.A. **116**, 14505 (2019).
[20] N. Li, Q. Huang, X. Y. Yue, W. J. Chu, Q. Chen, E. S. Choi, X. Zhao, H. D. Zhou, and X. F. Sun, Possible itinerant excitations and quantum spin state transitions in the effective spin-$\frac{1}{2}$ triangular-lattice antiferromagnet $Na_2BaCo(PO_4)_2$, Nat. Commun. **11**, 4216 (2020).
[21] Yuan Gao, Chuandi Zhang, Junsen Xiang, Dehong Yu, Xingye Lu, Peijie Sun, Wentao Jin, Gang Su, and Wei Li, Double magnon-roton excitations in the triangular-lattice spin supersolid, Phys. Rev. B **110**, 214408 (2024).
[22] J. Sakurai, W. J. L. Buyers, R. A. Cowley, and G. Dolling, Crystal dynamics and magnetic excitations in cobaltous oxide, Phys. Rev. **167**, 510 (1968).
[23] R. A. Cowley, W. J. L. Buyers, C. Stock, Z. Yamani, C. Frost, J. W. Taylor, and D. Prabhakaran, Neutron scattering investigation of the $d-d$ excitations below the Mott gap of CoO, Phys. Rev. B **88**, 205117 (2013).
[24] P. M. Sarte, R. A. Cowley, E. E. Rodriguez, E. Pachoud, D. Le, V. García-Sakai, J. W. Taylor, C. D. Frost, D. Prabhakaran, C. MacEwen, A. Kitada, A. J. Browne, M. Songvilay, Z. Yamani, W. J. L. Buyers, J. P. Attfield, and C. Stock, Disentangling orbital and spin exchange interactions for Co^{2+} on a rocksalt lattice, Phys. Rev. B **98**, 024415 (2018).
[25] P. M. Sarte, M. Songvilay, E. Pachoud, R. A. Ewings, C. D. Frost, D. Prabhakaran, K. H. Hong, A. J. Browne, Z. Yamani, J. P. Attfield, E. E. Rodriguez, S. D. Wilson, and C. Stock, Spin-orbit excitons in CoO, Phys. Rev. B **100**, 075143 (2019).
[26] P. M. Sarte, C. Stock, B. R. Ortiz, K. H. Hong, and S. D. Wilson, Van vleck excitons in Ca_2RuO_4, Phys. Rev. B **102**, 245119 (2020).
[27] H. Lane, M. Songvilay, R. A. Ewings, and C. Stock, Excitonic transverse and amplitude fluctuations in noncollinear and charge-ordered $RbFe^{2+}Fe^{3+}F_6$, Phys. Rev. B **106**, 054431 (2022).
[28] H. Lane, P. M. Sarte, K. Guratinder, A. M. Arevalo-Lopez, R. S. Perry, E. C. Hunter, T. Weber, B. Roessli, A. Stunault, Y. Su, R. A. Ewings, S. D. Wilson, P. Böni, J. P. Attfield, and C. Stock, Spin-orbital correlations from complex orbital order in MgV_2O_4, Phys. Rev. Res. **5**, 043146 (2023).
[29] H. Lane, E. E. Rodriguez, H. C. Walker, Ch. Niedermayer, U. Stuhr, R. I. Bewley, D. J. Voneshen, M. A. Green, J. A. Rodriguez-Rivera, P. Fouquet, S.-W. Cheong, J. P. Attfield, R. A. Ewings, and C. Stock, Metastable antiphase boundary ordering in $CaFe_2O_4$, Phys. Rev. B **104**, 104404 (2021).
[30] E. Chan, H. Lane, J. Pásztorová, M. Songvilay, R. D. Johnson, R. Downie, J-W. G. Bos, J. A. Rodriguez-Rivera, S.-W. Cheong, R. A. Ewings, N. Qureshi, and C. Stock, Neutron scattering sum rules, symmetric exchanges, and helicoidal magnetism in $MnSb_2O_6$, Phys. Rev. B **107**, 144420 (2023).
[31] D. J. Brener, I. Rodriguez Mallo, H. Lane, J. A. Rodriguez-Rivera, K. Schmalzl, M. Songvilay, K. Guratinder, C. Petrovic, and C. Stock, Anisotropic excitonic magnetism from discrete C_4 symmetry in $CeRhIn_5$, Phys. Rev. B **110**, 064434 (2024).
[32] See Supplemental Material at http://link.aps.org/supplemental/10.1103/PhysRevLett.134.136703 for additional information on experiments and data parameterization.
[33] W. J. L. Buyers, T. M. Holden, and A. Perreault, Temperature dependence of magnetic excitations in singlet-ground-state systems. II. Excited-state spin waves near the curie temperature in Pr_3Tl, Phys. Rev. B **11**, 266 (1975).
[34] M. T. F. Telling and K. H. Andersen, Spectroscopic characteristics of the OSRIS near-backscattering crystal analyser spectrometer on the ISIS pulsed neutron source, Phys. Chem. Chem. Phys. **7**, 1255 (2005).
[35] F. Demmel and K. Pokhilchuk, The resolution of the tof-backscattering spectrometer osiris: Monte Carlo simulations and analytical calculations, Nucl. Instrum. Methods Phys. Res., Sect. A **767**, 426 (2014).
[36] C. Stock, C. Broholm, Y. Zhao, F. Demmel, H. J. Kang, K. C. Rule, and C. Petrovic, Magnetic field splitting of the spin resonance in $CeCoIn_5$, Phys. Rev. Lett. **109**, 167207 (2012).
[37] C. Stock, C. Broholm, F. Demmel, J. Van Duijn, J. W. Taylor, H. J. Kang, R. Hu, and C. Petrovic, From incommensurate correlations to mesoscopic spin resonance in $YbRh_2Si_2$, Phys. Rev. Lett. **109**, 127201 (2012).
[38] N. Kernavanois, E. Ressouche, P. J. Brown, Y. J. Henry, and E. Lelievre-Berna, Magnetization distribution in paramagnetic nickel and cobalt oxides, Physica B (Amsterdam) **350**, E265 (2004).
[39] N. Kernavanois nd E. Ressouche, P. J. Brown, Y. J. Henry, and E. Lelievre-Berna, Magnetization distribution in paramagnetic CoO: A polarized neutron diffraction study, J. Phys. Condens. Matter **15**, 3433 (2003).
[40] M. E. Zhitomirsky and A. L. Chernyshev, Colloquium: Spontaneous magnon decays, Rev. Mod. Phys. **85**, 219 (2013).

[41] T. Masuda, A. Zheludev, H. Manaka, L.-P. Regnault, J.-H. Chung, and Y. Qiu, Dynamics of composite haldane spin chains in IPA-$CuCl_3$, Phys. Rev. Lett. **96**, 047210 (2006).
[42] H. E. Stanley, *Introduction to Phase Transitions and Critical Phenomena* (Oxford University Press, Oxford, 1971).
[43] R. K. Wehner and E. F. Steigmeier, Coupled lattice modes in light scattering, RCA Rev. **36**, 70 (1975).
[44] J. Magarino, J. Tuchendler, A. R. Fert, and J. Gelard, Field dependence of uniform magnon energies in lamellar $CoCl_2$ and $CoBr_2$ by AFMR experiments, Solid State Commun. **23**, 175 (1977).
[45] Ch. Rüegg, B. Normand, M. Matsumoto, A. Furrer, D. F. McMorrow, K. W. Krämer, H. U. Güdel, S. N. Gvasaliya, H. Mutka, and M. Boehm, Quantum magnets under pressure: Controlling elementary excitations in $TlCuCl_3$, Phys. Rev. Lett. **100**, 205701 (2008).
[46] R. Coldea, D. A. Tennant, E. M. Wheeler, E. Wawrzynska, D. Prabhakaran, M. Telling, K. Habicht, P. Smeibidl, and K. Kiefer, Quantum criticality in an Ising chain: Experimental evidence for emergent E_8 symmetry, Science **327**, 177 (2010).